Environmental Health Perspectives
Vol. 84, pp. 83-94, 1990

Multiparameter Digitized Video Microscopy of Toxic and Hypoxic Injury in Single Cells

John. J. Lemasters,* Gregory J. Gores,* Anna-Liisa Nieminen,* Thomas L. Dawson,* Barnaby E. Wray,* and Brian Herman*

There is no clear picture of the critical events that lead to the transition from reversible to irreversible injury. Many studies have suggested that a rise in cytosolic free Ca^{2+} initiates plasma membrane bleb formation and a sequence of events that lead ultimately to cell death. In recent studies, we have measured changes in cytosolic free Ca^{2+}, mitochondrial membrane potential, cytosolic pH, and cell surface blebbing in relation to the onset of irreversible injury and cell death following anoxic and toxic injury to single hepatocytes by using multiparameter digitized video microscopy (MDVM). MDVM is an emerging new technology that permits single living cells to be labeled with multiple probes whose fluorescence is responsive to specific cellular parameters of interest. Fluorescence images specific for each probe are collected over time, digitized, and stored. Image analysis and processing then permits quantitation of the spatial distribution of the various parameters with the single living cells. Our results indicate the following: The formation of plasma membrane blebs accompanies all types of injury in hepatocytes. Cell death is a rapid event initiated by rupture of a plasma membrane bleb, and it is coincident with the onset of irreversible injury. An increase of cytosolic free Ca^{2+} is not the stimulus for bleb formation or the final common pathway leading to cell death. A decrease of mitochondrial membrane potential precedes the loss of cell viability. Cytosolic pH falls by more than 1 pH unit during chemical hypoxia. This acidosis protects against the onset of cell death.

Introduction

Until recently, research on hypoxic and toxic cell injury was, almost without exception, directed towards large populations of cells (e.g., whole tissue, cell suspensions, cell cultures). However, in such preparations, the onset of irreversible injury is not synchronous. Following hypoxia for example, minutes or even hours can even pass between death of the first cell in a population and the last cell. Thus, the events that lead to irreversible injury and cell death are obscured when whole cell populations are studied, especially if these events occur rapidly or suddenly. The determination of the temporal sequence of such rapidly occurring events may simply be impossible.

We are attempting to overcome these drawbacks by measuring multiple cellular functions in individual cells during toxic and hypoxic injury by using multiparameter digitized video microscopy (MDVM). With this new, rapidly developing technology, we are monitoring, on a quantitative basis, a number of basic cellular processes with high temporal resolution, including cytosolic free Ca^{2+}, cytosolic pH, mitochondrial membrane potential, lysosomal integrity and pH, plasmalemmal permeability, cell surface morphology, and cell viability. Our data show that MDVM can provide fundamental new information about hypoxic and toxic injury in living cells that is unobtainable by any other technique.

Multiparameter Digitized Video Microscopy

Configuration of the MDVM System

Our MDVM system is comprised of a Zeiss IM-35 inverted microscope equipped with UV-transmitting phase contrast optics, xenon or mercury lamp epi-illumination, an MTI DAGE Model 66 intensified silicon-intensified target (ISIT) camera, a Digital Equipment minicomputer containing an analog to

*Laboratories for Cell Biology, Department of Cell Biology and Anatomy, School of Medicine, University of North Carolina at Chapel Hill, Chapel Hill, NC 27599.

Address reprint requests to J. Lemasters, Laboratories for Cell Biology, Department of Cell Biology and Anatomy, School of Medicine, University of North Carolina at Chapel Hill, Chapel Hill, NC 27599.

digital converter and frame memories from Imaging Technologies, a time-lapse video cassette recorder from RCA, computer-driven filter wheels for changing excitation and emission light, and software for image processing and analysis (*1*). The high sensitivity of the ISIT camera, together with the frame averaging capability of the computer, allows us to work at very low levels of excitation energy and fluorophore concentration, thus preventing photobleaching or photodamage that might lead to disruption of normal cell activity. The ISIT camera can also be used to obtain bright field images, allowing the acquisition of phase and fluorescent images from the same cells. In a typical experiment, we monitor and record phase-contrast images continuously at low illumination with brief interruptions to collect digitized fluorescent images. With the phase-contrast images, we can see changes in cell structure that are then correlated with quantitative changes in the fluorescent images.

Fluorescent Probes of Cellular Functions

The experimental approach we follow takes advantage of the availability of a number of different fluorescent compounds whose excitation and emission spectra are sensitive to various environmental parameters and which preferentially accumulate into different subcellular compartments in intact living cells. This enables us to study multiple cellular functions in individual living cells in response to external stimuli.

For the studies reviewed here, we used Fura-2 to measure free Ca^{2+} (*2*), rhodamine 123 to monitor mitochondrial membrane potential (*3,4*), BCECF to determine intracellular pH (*5*), and propidium iodide to label the nuclei of nonviable cells (*6*). When excited at 340 or 350 nm, the fluorescence of Fura-2 shows a dependence on Ca^{2+} concentration with a K_d of about 225 nM; when excited at 362 nm (isoasbestic point), there is no change in fluorescence intensity with a change in Ca^{2+}. Corresponding pH-sensitive and pH-insensitive wavelengths for BCECF are 490 and 440 nm. Rhodamine 123 has been extensively employed as a fluorescent label of mitochondria and distributes electrophoretically in response to the mitochondrial membrane potential (*4*). Propidium iodide has seen widespread use in flow cytometry and labels nonviable cells exactly like trypan blue.

Fluorescence specific to each probe is selected, employing the appropriate excitation and emission filters. In preparations loaded with several fluorophores, multiple parameters can be monitored quantitatively over time in single living cells. Introducing this multiparameter technique in 1985 (*7*), we showed that four or more variables of interest can be monitored in the same cell sequentially by selecting parameter-specific fluorophores with nonoverlapping emission and excitation spectra.

Ratio Imaging

The use of MDVM not only provides quantitative information regarding the amount of fluorophore emission, but also the spatial and temporal characteristics of this emission. However, because MDVM provides a two-dimensional image of a three-dimensional object (i.e., the cell), misleading estimates of the fluorophore concentration in different parts of the cell will be obtained due to differences in pathlength or accessible volume (Fig. 1). To correct for this problem, images are acquired from cells at two different excitation wavelengths, one that is parameter sensitive and one that is not. By dividing the images obtained at both wavelengths, errors introduced by differences of pathlength, regional fluorophore concentration, dye leakage over time, photobleaching, and accessible volume are corrected. Such ratio imaging is employed with Fura-2 to determine cytosolic free Ca^{2+} and with BCECF to determine cytosolic pH.

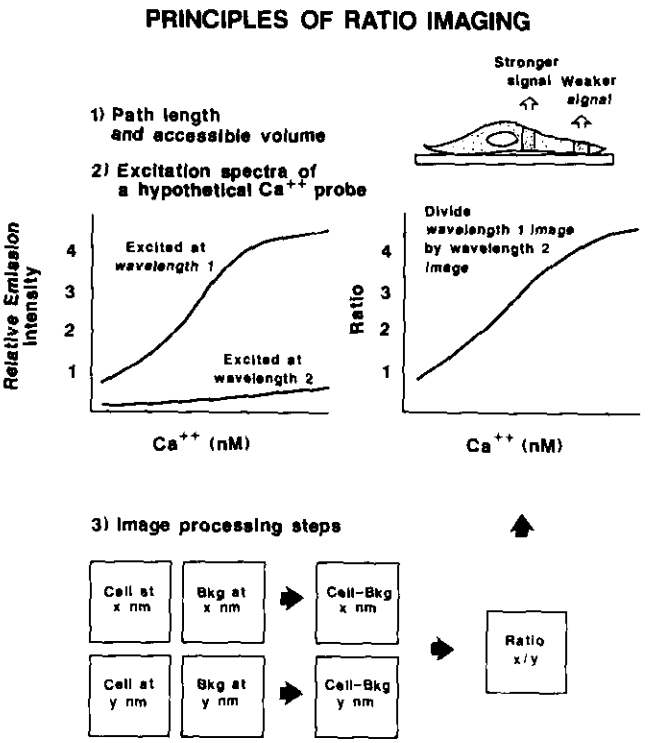

FIGURE 1. Principles of ratio imaging. Fluorophore emission can be a selective indicator of environmental factors. Fura-2 fluorescence is sensitive to free Ca^{2+} but also to pathlength and accessible volume (as illustrated in 1). Ratio imaging can correct for these factors (as illustrated in 2). Fura-2 is excited at two different wavelengths, one that excites Ca^{2+}-sensitive fluorescence and the other which excites Ca^{2+}-insensitive fluorescence. The ratio of Ca^{2+}-sensitive to Ca^{2+}-insensitive fluorescence is proportional to Ca^{2+} concentration, and errors due to pathlength, Fura-2 concentration, and accessible volume are factored out. As illustrated in 3, ratio imaging on a pixel-by-pixel basis using our MDVM system produces a two-dimensional map of free Ca^{2+} concentration. Background images are obtained at each wavelength and are subtracted from the experimental images at each wavelength before ratioing. Once ratioed, Ca^{2+} concentration is determined by comparison to a standard curve stored in computer memory.

Table 1. Problems associated with Fura-2 and other probes.

Problem	Test	Solution
Incomplete ester hydrolysis during loading	Determine spectra and parameter sensitivity of probe from detergent extracted cells	Microinjection, scrape loading, ATP permeabilization, etc.
Sequestration into organelles	Monitor loss of probe as subcellular compartments are opened with graded concentrations of detergent	Microinjection, scrape loading, ATP permeabilization, etc.
Spectral shifts as function of viscosity, pH, or polarity	Determine spectra as function of microviscosity, pH, and solvent polarity	Ratio with respect to an isoasbestic wavelength
Changes of K_d as function of viscosity, pH, or polarity	Determine K_d as function of microviscosity, pH, and solvent polarity	Make appropriate correction
Dye leakage from cells	Monitor dye leakage at isoasbestic wavelength	Use multiple-charged probes
Photobleaching, photochemical alterations, phototoxicity.	Monitor at isoasbestic wavelength; determine spectra after detergent extraction	Attenuate excitation < 1000-fold; use stable probes

Problems Associated with Fura-2 Measurements of Free Ca^{2+}

Fura-2 and BCECF are loaded as their acetoxymethyl esters (5 μM for 30 min in growth medium). Cytoplasmic esterases serve to cleave the acetoxymethyl ester bonds, releasing free Fura-2 or BCECF into the cytosol at concentrations in the range of 50 to 200 μM. Several technical issues concern the use of Fura-2 and BCECF. As summarized in Table 1 for Fura-2, these include: *a*) incomplete ester hydrolysis (*8*); *b*) sequestration into organelles (*9–12*); *c*) shifts in excitation and emission spectra and K_d for Ca^{2+} dependent on viscosity, pH, polarity, and other factors (*9,13*); *d*) dye leakage from cells; and *e*) photochemical formation of fluorescent, Ca^{2+}-insensitive derivatives of Fura-2 (*14*).

All of these concerns are important, and Table 1 summarizes how each concern is addressed. However, the sequestration of Fura-2 into organelles is possibly most critical for correct qualitative interpretation of the data. For this reason, we have recently developed a definitive technique for the subcellular localization of Fura-2 and related dyes using MDVM (*15,16*). The principle of the approach is to co-load cells with Fura-2 (or other dye of interest) and additional fluorescent probes that are specific for various subcellular compartments: rhodamine 123 for mitochondria, rhodamine-dextran for lysosomes, and rhodamine microspheres (0.1 μm) for the pre-lysosomal endocytic compartment. Rhodamine-dextran is pulse-loaded a day earlier, and rhodamine 123 and rhodamine microspheres are co-loaded with the other dye of interest. In the multiply labeled cells, various compartments are sequentially opened by increasing concentrations of digitonin. A Ca^{2+}-free, succinate-containing buffer is employed to prevent mitochondrial depolarization after permeabilization of the plasma membrane. As illustrated for hepatocytes loaded with BCECF, 20 μM digitonin opens the cytosol but leaves mitochondria (Fig. 2), endosomes (Fig. 3), and lysosomes (Fig. 4) intact. The subsequent additon of 100 μM digitonin opens the lysosomal and endosomal compartments,

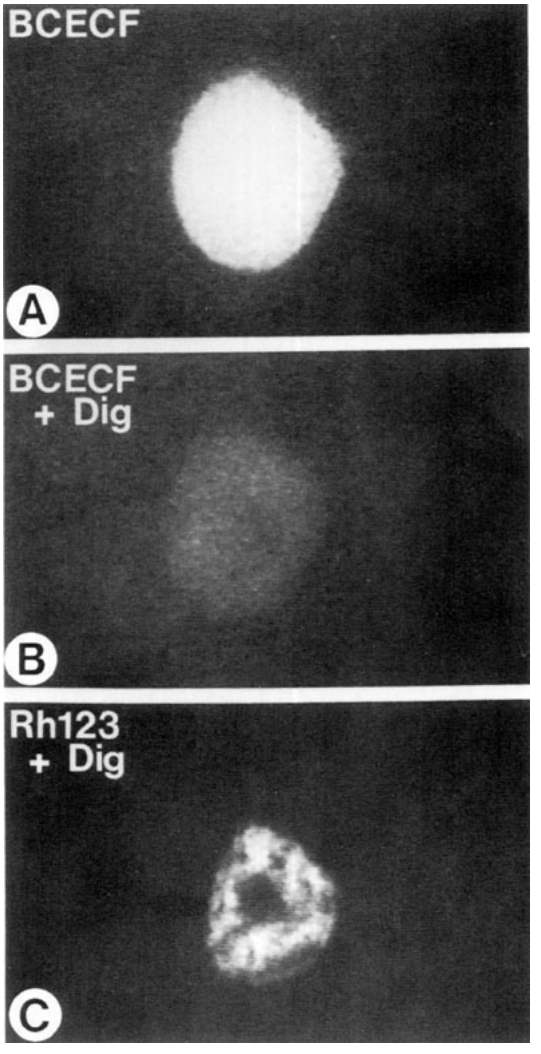

FIGURE 2. Subcellular localization of BCECF by MDVM: mitochondria. A cultured hepatocyte was loaded with BCECF and displayed diffuse fluorescence (*A*). After addition of 100 μM digitonin in succinate-containing Ca^{2+}-free buffer, virtually all BCECF fluorescence disappeared (*B*). Rhodamine 123 was subsequently added to identify mitochondria (*C*). This experiment demonstrates the absence of significant mitochondrial loading by BCECF.

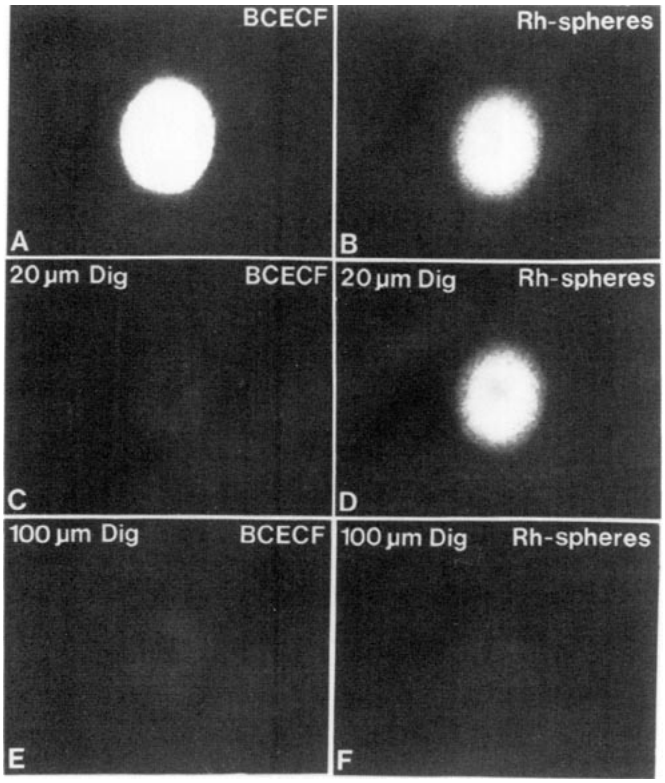

FIGURE 3. Subcellular localization of BCECF by MDVM: endosomes. A cultured hepatocyte was loaded with both BCECF and 0.1 μm rhodamine-labeled-latex microspheres. The cell was diffusely labeled with both probes (*A*, *B*). After 20 μM digitonin, virtually all BCECF fluorescence was released (*C*), but rhodamine-microsphere fluorescence remained intact (*D*). After 100 μM digitonin (conditions that do not disrupt mitochondria; see Fig. 2), no additional loss of BCECF fluorescence occurred (*E*), but rhodamine-microsphere fluorescence disappearance was complete (*F*). This experiment demonstrates the absence of BCECF localization to diffuse prelysosomal endocytic compartment.

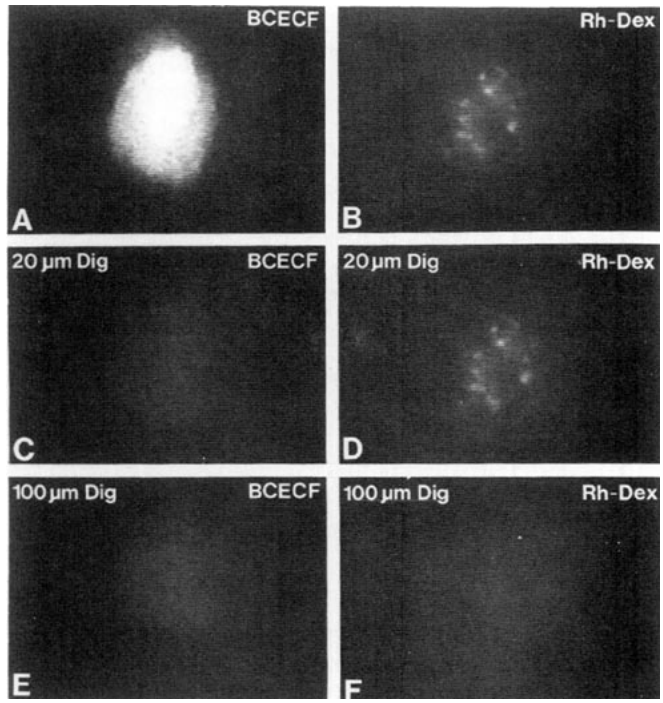

FIGURE 4. Subcellular localization of BCECF by MDVDM: lysosomes. A hepatocyte was loaded with rhodamine-dextran 48 hr earlier by IP injection. After 1 day in culture, the cell was loaded additionally with BCECF. BCECF fluorescence from the cell was diffuse (*A*); whereas rhodamine-dextran fluorescence was punctate consistent with its localization to secondary lysosomes (*B*). After 20 μM digitonin, virtually all BCECF fluorescence was released (*C*), but rhodamine-dextran was unchanged (*D*). After 100 μM digitonin, no additional loss of BCECF fluorescence occurred (*E*), but rhodamine-dextran fluorescence was lost entirely (*F*). This experiment demonstrates the absence of BCECF localization to lysosomes. Since 20 μM digitonin released BCECF completely, but left lysosomes, endosomes, mitochondria, and presumably other membranous organelles intact, it can be concluded that BCECF was localized exclusively to the cytosol (including nucleoplasm).

but mitochondria are preserved. More digitonin or another detergent (e.g., Triton X-100) releases the remaining mitochondrial fluorescence. From such experiments, we have quantitated the extent and amount of co-localization of Fura-2 in noncytosolic compartments from the digital images. In hepatocytes, we have had success in loading Fura-2 and BCECF with greater than 85% specificity for cytosol and less than 10% accumulation in the mitochondria or lysosomes. Our loading protocol also results in virtually complete hydrolysis of Fura-2-AM to Fura-2. However, the results from other cell types (e.g., cardiac myocytes, vascular smooth muscle cells, fibroblasts) can be quite different (*9*); thus it is essential to evaluate Fura-2 compartmentation in each new cell type studied.

Experimental Models of Cell Injury

We have used four different protocols to produce toxic or anoxic injury in 24-hr cultured rat hepatocytes. True anoxia was established by perfusing an environmental chamber mounted on the stage of the microscope with medium containing 1 mg protein/mL submitochondrial particles and 5 mM succinate (*17*). Submitochondrial particles consume oxygen quantitatively just as tissue does in ischemia. Because the submitochondrial particles were premixed with the medium, anoxia was established as soon as the medium containing succinate and the submitochondrial particles was perfused into the chamber. KCN (2.5 mM) and iodoacetate (0.5–10 mM) were employed to inhibit ATP production by oxidative phosphorylation and glycolysis (*6,16,18*). This treatment mimics the fall in ATP that accompanies anoxia and is termed chemical hypoxia. $HgCl_2$ (50 μM) was used to attack membrane transport processes (toxic injury), and cystamine (5 mM) was employed to cause oxidative stress by forming mixed disulfides with plasma membrane thiols (*19,20*).

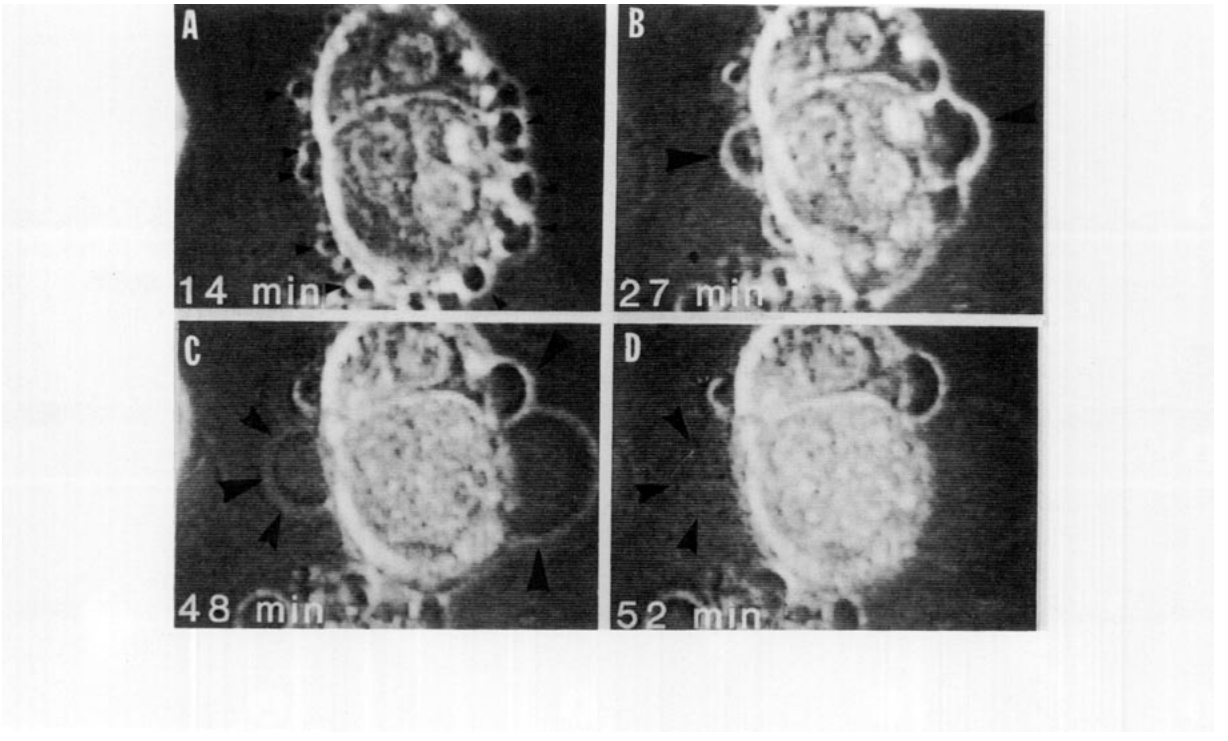

FIGURE 5. Stages of bleb formation. Three stages of bleb development were identified in cultured hepatocytes after metabolic inhibition with KCN plus iodoacetate (chemical hypoxia). Stage 1 was formation of numerous small blebs (*A*, arrowheads) within 15 min. Stage 2 began after about 20 to 25 min and involved the growth and coalescence of adjacent blebs (*B*, arrowheads) that continued to grow until a few large terminal blebs were formed (*C*). Stage 3 was rupture of one of the terminal blebs (note absence of large bleb on left in *D*). Elapsed time from initiation of chemical hypoxia is shown in the lower left corner.

Role of Cell Surface Blebbing in Cell Death

Stages of Bleb Formation

Bleb formation occurred in all the experimental treatments (*6,7,16,17,19,20*). Three stages could be recognized. Stage 1 consisted of numerous small surface blebs (Fig. 5*A*). In chemical hypoxia, stage 1 blebbing began within 10 min of addition of KCN and IAA. Stage 2 began after about 20 min. During stage 2, blebs grew through a process of coalescence and bleb fusion (Fig. 5*B*) until one to three large terminal blebs were left (Fig. 5*C*). Bleb enlargement was a slow process requiring minutes. Bleb fusion was extremely rapid and occurred within consecutive video frames (33 msec; data not shown). Stage 3 of blebbing was initiated by rupture of one of the terminal belbs (Fig. 5*D*). Blebs were phase-lucent during all stages, indicating the absence of granular organelles such as mitocondria and lysosomes. The time required for progression of cells through stages 1 and 2 varied from cell to cell and depended on the type of injury. Thus, determination in single cells of bleb progression in relation to alterations in other cellular paarameters was essential for our studies.

Onset of Irreversible Injury

Alterations in the structure and function of the plasma membrane have received attention as a major focus in the evolution of hypoxic damage and in the transition from reversible to irreversible injury. Our results demonstrate direct plasma membrane injury in the form of bleb formation and eventual bleb rupture. Bleb rupture precipitates the onset of cell death, but the transition from reversible to irreversible injury may occur earlier. Therefore, we undertook a study to document the onset of irreversible injury with respect to plasma membrane blebbing, bleb rupture, and onset of cell death (*17*). Our strategy was to reoxygenate anoxic hepatocytes at various stages of blebbing and determine at what point the injury was no longer reversible.

Cells were made anoxic by incubating them on the microscope stage with submitochondrial particles and succinate. Reoxygenation was achieved by the infusion of fresh, oxygenated medium that did not contain submitochondria particles or succinate. When cells in stages 1 or 2 of bleb development were reoxygenated, their blebs were resorbed (Fig. 6*A-L*). There was no apparent reoxygenation injury, and the hepatocytes continued to exclude propidium iodide (Fig. 6*D* and *H*). However, in stage 3 cells that had already taken

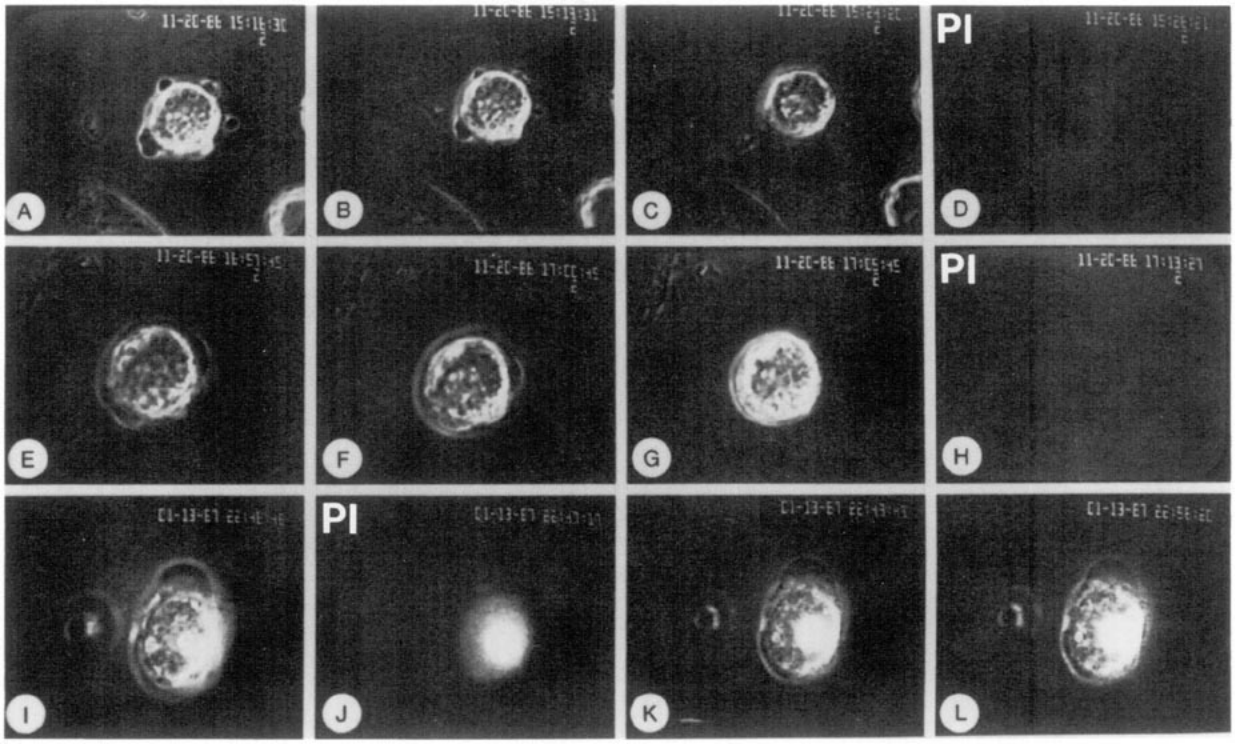

FIGURE 6. Reoxygenation of anoxic hepatocytes: reversibility of bleb formtion. Anoxic hepatocytes from 24-hr fasted rats were reoxygenated by infusion of oxygenated medium via a syringe pump. Reoxygenation required about 2 min (function of infusion rate and the dead space of the system). (*A-D*): a hepatocyte after 25 min of anoxia was in stage 1 of blebbing (*A*). After about 1 min of reoxygenation (*B*), blebs were beginning to be resorbed. After about 6 min of reoxygenation (*C*), blebs had resorbed and propidium iodide was still excluded (*D*). (*E–H*): a hepatocyte after 60 min of anoxia was in stage 2 of blebbing (*E*). After about 1 min of reoxygenation, blebs were resorbing (*F*). After 6 min of reoxygenation, blebs had resorbed (*G*) and the cell continued to be viable by the criteria of propodium iodide exclusion (*H*). (*I-L*): a hepatocyte after 406 min of anoxia was in stage 3 of injury (*I*) and had lost viability as indicated by propidium iodide uptake (*J*). Reoxygenation after about 1 min (*K*) or 6 min (*L*) did not reverse bleb formation or other changes in morphology.

up propidium iodide as a consequence of bleb lysis, reoxygenation did not reverse bleb formation or lead to any other change in cell structure (Fig. 6*I-L*). Thus in anoxic hepatocytes, the onset of cell death and the transition from reversible to irreversible injury appeared to occur at the same time.

Bleb Rupture

Scanning electron microscopy was used to characterize changes in membrane structural integrity after bleb lysis or rupture. A field of cells was viewed in the video microscope during chemical hypoxia. Blebs formed (Fig. 7*a*) and after the first bleb had ruptured in one of the cells (Fig. 7*b*), propidium iodide uptake by the cell was documented (Fig. 7*c*), and the coverslip was flooded with fixative and prepared for scanning electron microscopy (Fig. 7*d*). In cells not taking up propidium iodide, the cell surface was smooth and continuous with large, intact blebs (cell on the left in Fig. 7*d*). In the cell which had lost viability, a large discontinuity of the membrane surface was observed; it was rimmed by vesiculated fragments of membrane (cell on the right in Fig. 7*d*). Thus, bleb rupture led literally to a large hole in the plasma membrane.

Chemical Hypoxia

Cytosolic Free Ca^{2+} during Chemical Hypoxia

It has been suggested that a rise in cytosolic free Ca^{2+} initiates a series of harmful processes that culminate in cell death (*21-24*). Using MDVM and ratio imaging of Fura-2 fluorescence, we monitored cytosolic free Ca^{2+} following chemical hypoxia with KCN plus iodoacetate in relation to mitochondrial membrane potential, bleb formation, and the onset of cell death (Fig. 8). Unexpectedly, chemical hypoxia was not associated with any change in cytosolic free Ca^{2+} up to the point of cell death, even though these cells underwent blebbing.

To document that Fura-2 in these cells was responsive to change in cytosolic free Ca^{2+}, hepatocytes were treated with vasopressin, phenylephrine, and an epidermal growth factor—all of which increased free Ca^{2+}, as measured by Fura-2 ratio imaging (*6*). Ionomycin, a calcium ionophore, also increased free Ca^{2+}, whereas addition of EGTA, which chelates extracellular free calcium, caused a slight decrease. Thus, Fura-2 responded to stimuli that both increased and

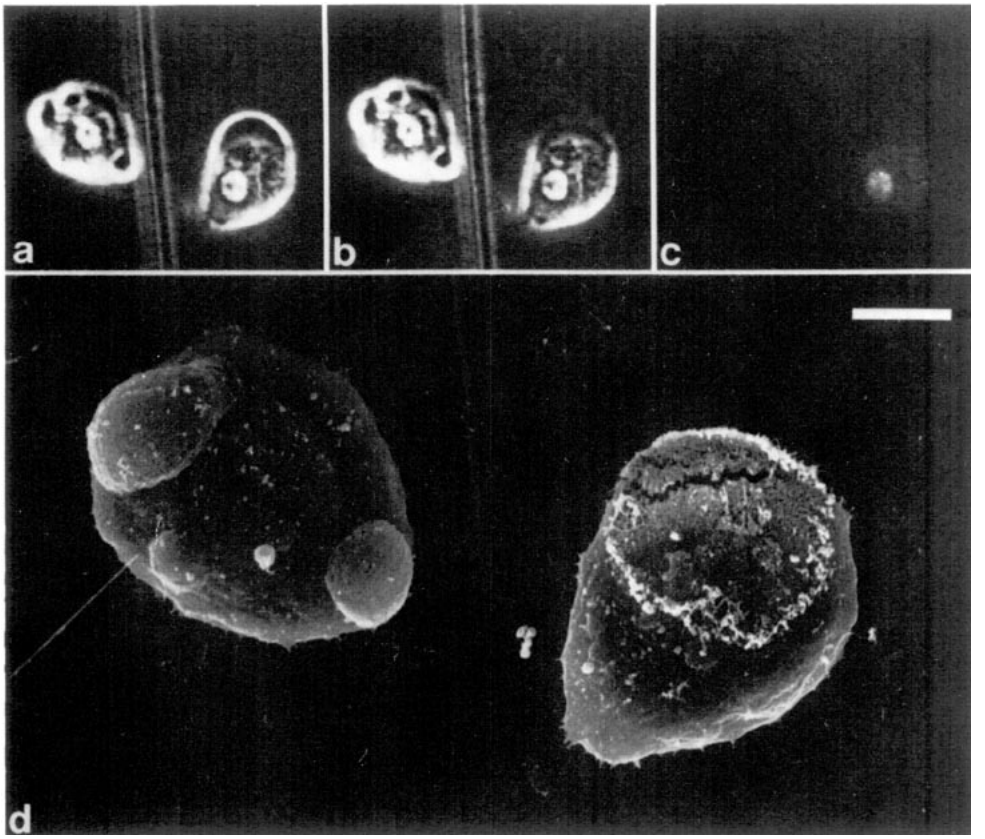

FIGURE 7. Scanning electron microscopy of ruptured bleb. After about 50 min of chemical hypoxia, terminal blebs had formed on two cells (*A*). After 200 msec (one video frame in the time-lapse recording) the terminal bleb on the cell to the right had ruptured (*B*), and several sec later this cell was labeled with propidium iodide (*C*). The cell to the left continued to exclude the fluorescent dye. The preparation was then fixed and prepared for scanning electron microscopy (*D*). A large surface discontinuity bordered by small membrane vesicles was observed after bleb rupture in the cell to the right. The surface of the cell to the left was smooth and continuous. Bar is 10 μM.

decreased cytosolic free Ca^{2+}. Although substantial increases in free Ca^{2+} were caused by these hormones, cells die not bleb and remained viable for long periods of time. In addition, we determined in multiple labeling experiments nearly all the internalized Fura-2 was nonmitochondrial and nonlysosomal (*15*). Moreover, the fluorescence spectrum of Fura-2 released from cells by detergent was nearly identical to that of the pure Fura-2 free acid in the same buffer and was fully responsive to Ca^{2+}, indicative of the absence of unhydrolyzed or partially hydrolyzed Fura-2-AM.

Mitochondrial Membrane Potential during Chemical Hypoxia

Anoxic injury is initiated by an inhibition of ATP synthesis leading to a lack of energy supply for cellular reactions. Mitochondria serve as the primary site of ATP synthesis, and synthesis of ATP is associated with the generation of a potential difference across the mitochondrial inner membrane. Rhodamine 123 is a fluorescent dye that accumulates electrophoretically in mitochondria in response to the potential difference across the inner membrane (*4*). Following chemical hypoxia, the mitochondrial membrane potential decreased steadily, concomitant with bleb formation until the onset of cell death (Fig. 8) (*6*). After loss of cell viability, a large final drop in potential occurred and rhodamine 123 fluorescence could no longer be measured above background. Before bleb rupture, the potential decreased about 30 mV or 20% of the initial potential of 160 mV (*25*). A similarly persisting potential has been reported in hepatocyte suspensions during anoxia (*26*).

Cytosolic pH and Cell Injury

Acidosis is a salient feature of ischemic tissue injury. Accordingly, we measured intracellular pH (pH_i) in 24-hr cultured rat hepatocytes by ratio imaging of BCECF fluorescence using MDVM (*16*). In normoxic cells, pH_i closely followed changes of pH_o. Following chemical hypoxia at pH_o of 7.4, pH_i decreased by more than a unit within 10 min after the addition of the metabolic inhibitors (Fig. 9). There was little spatial heterogeneity of pH_i in either normoxic or hypoxic cells (Fig. 10). After 20 to 30 min, pH_i began to rise, and cell death, as indicated by propidium iodide nuclear staining, ensued after

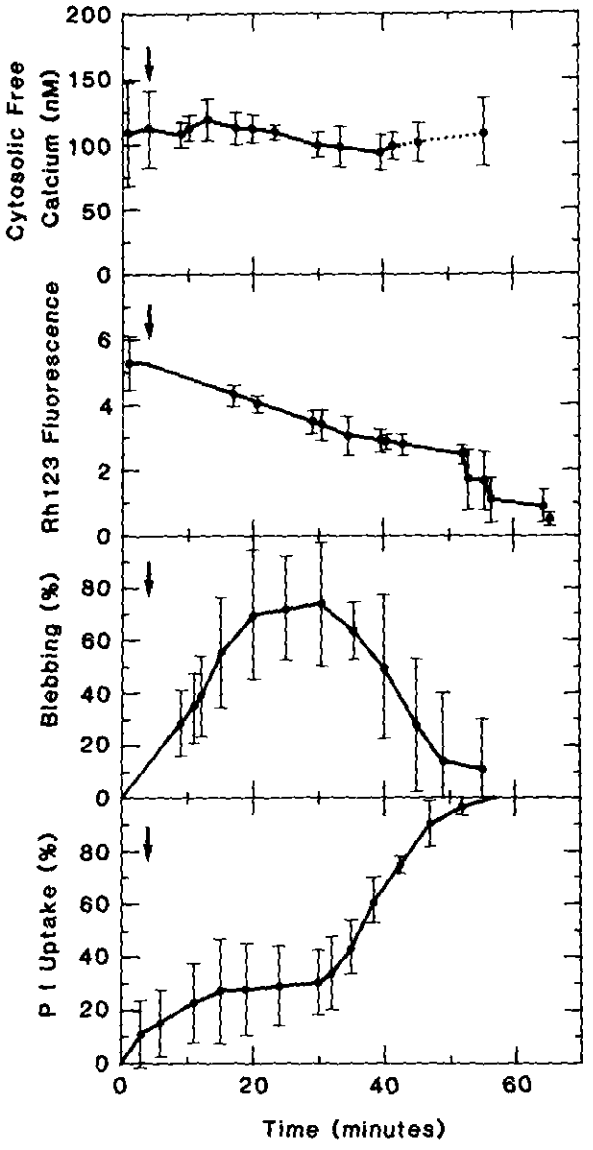

FIGURE 8. Changes in cytosolic free Ca^{2+}, rhodamine 123 fluorescence, cell surface blebbing, and propidium iodide uptake after chemical hypoxia in cultured hepatocytes. Hepatocytes were labeled with Fura-2 and rhodamine 123 and incubated in propidium iodide-containing medium. Arrow indicates addition of KCN and iodoacetate to initiate chemical hypoxia. Cytosolic free Ca^{2+} was measured by Fura-2 ratio imaging. Rhodamine 123 (Rh123) fluorescence reflects mitochondrial membrane potential, and propidium iodide uptake indicates loss of cellular viability. Dotted line (upper panel) indicates first loss of Fura-2 in individual experiments.

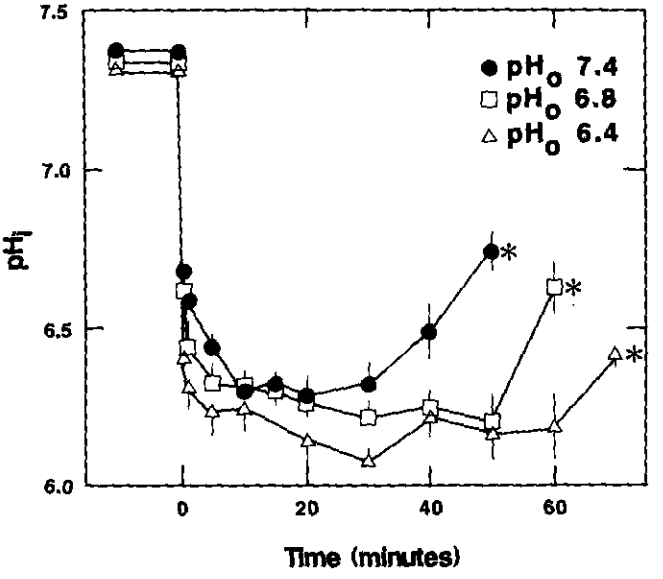

FIGURE 9. Cytosolic pH (pH_i) in single cultured hepatocytes during chemical hypoxia at different extracellular pH (pH_o). pH_o was changed simultaneously with the addition of cyanide and iodoacetate. pH_i was measured by ratio imaging of BCECF fluorescence using MDVM. Asterisks (*) indicate cell death as evidenced by loss of BCECF fluorescence at the pH-insensitive wavelength.

another 10 min (Figs. 9 and 10). At acidic pH_o (Fig. 9) or when Na^+/H^+ exchange was inhibited with choline (Fig. 11), pH_i decreased to similar values during chemical hypoxia, but the duration of intracellular acidosis was prolonged an additional 20 to 30 min. Cell survival was prolonged to a similar degree. Monensin prevented an acidic pH_i from forming and accelerated the onset of cell death (Fig. 11). ATP depletion measured in cell suspensions at neutral and acidic pH_o was identical and could not explain the prolonged cell survival (*18*).

These results indicate that intracellular acidosis develops rapidly in hepatocytes during ATP depletion, but pH_i rises shortly before cell death. Inhibiting Na^+/H^+ exchange or placing cells in an acidic pH_o prolongs intracellular acidosis and delays the onset of irreversible injury. Thus, intracellular acidosis protects against cell death from ATP depletion—a phenomenon that may represent a protective adaptation against hypoxic and ischemic stress.

Toxic and Oxidative Injury

Cytosolic Free Ca^{2+} during Toxic Injury with $HgCl_2$ and Cystamine

In contrast to chemical hypoxia, exposure of cells to $HgCl_2$ resulted in a large increase in free Ca^{2+}, and the cells died more rapidly (Fig. 12) (*19,20*). Bleb formation was also rapid and actually preceded the rise in calcium (Fig. 12, arrow, top panel). A spatial gradient of calcium also developed in these cells with blebs having higher concentrations of free Ca^{2+} (exceeding 1 μM) than the rest of the cell (Fig. 13). The source of this increased Ca^{2+} was extracellular, since in low Ca^{2+} medium, cytosolic free Ca^{2+} did not change after $HgCl_2$. The rate of cell killing, however, was unchanged.

Bleb formation also occurred in cells exposed to

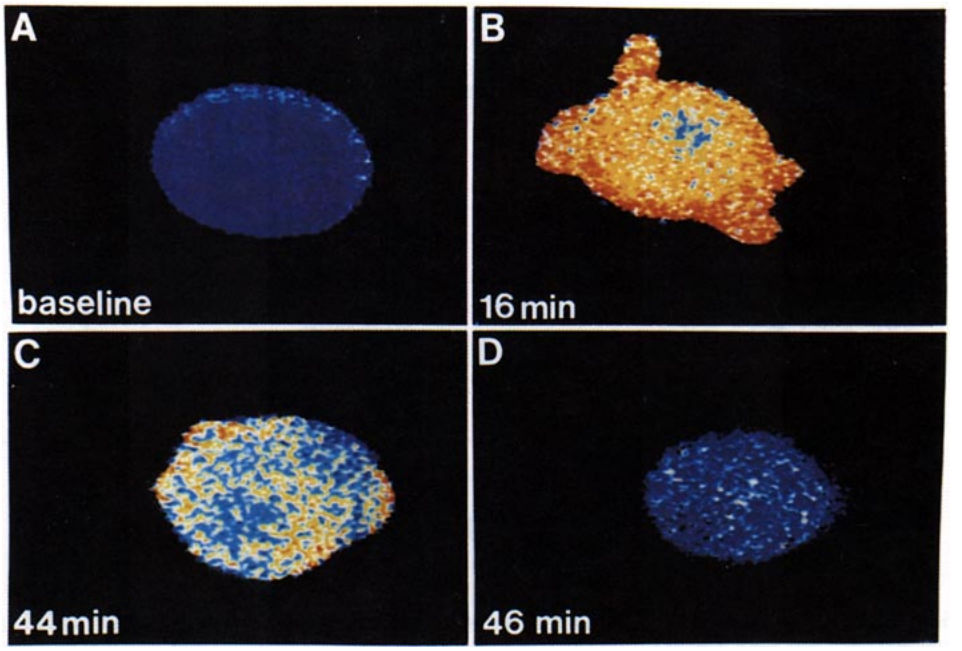

FIGURE 10. Pseudocolor maps of cytosolic pH during chemical hypoxia. pH_i was measured in a single, cultured hepatocyte after exposure to KCN plus iodacetate using MDVM and ratio imaging of BCECF fluorescence. Basal pH_i was 7.4 before metabolic inhibition, as represented by blue (*A*). After 16 min of chemical hypoxia, pH_i averaged 6.4 as displayed in orange and red (*B*). After about 44 min, pH_i began to increase as shown by mixed orange and blue (*C*). After 46 min, pH_i was 7.1 (*D*). Two minutes later the cell was dead, and BCECF fluorescence was below threshold.

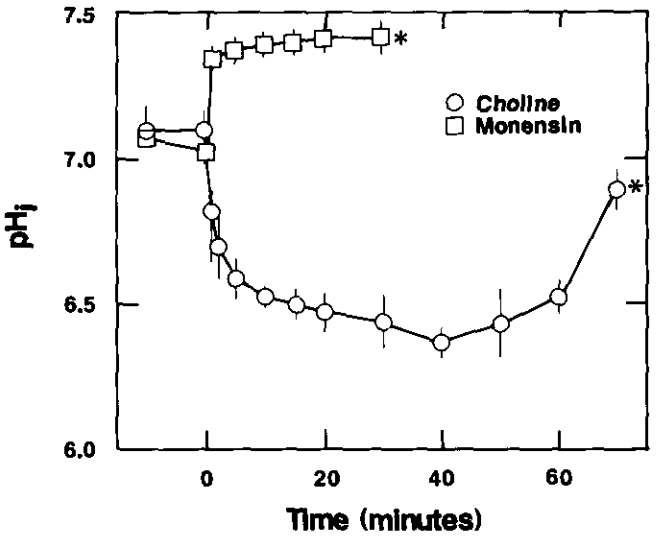

FIGURE 11. Effect on pH_i of inhibition or promotion of Na^+/H^+ exchange in single cultured rat hepatocytes during chemical hypoxia. KCN and iodoacetate were added at zero time simultaneously with either choline replacement for Na^+ to inhibit Na^+/H^+ exchange or monensin to enhance Na^+/H^+ exchange. Asterisks (*) indicate the onset of cell death.

cystamine with bleb rupture occurring after 40 to 70 min (*20*). Similar to chemical hypoxia, cytosolic free Ca^{2+} did not increase prior to blebbing or the onset of cell death (Fig. 12) nor did any spatial heterogeneity of Ca^{2+} concentration develop (Fig. 13). These studies demonstrate that a rise in cytosolic free Ca^{2+} is not a prerequisite for bleb formation or the final common pathway to cell death.

Mitochondrial Membrane Potential

A decrease of rhodamine 123 fluorescence also occurred early in $HgCl_2$ toxicity and actually preceded any change in free Ca^{2+} (Fig. 14). The half-maximal decrease of fluorescence occurred after about 6 min in both low and high Ca^{2+} mediums. Redistribution of rhodamine 123 fluorescence from mitochondrial to cytosolic compartments preceded the decrease of total cellular rhodamine 123 fluorescence (Fig. 15), indicating an even earlier collapse of the mitochondrial membrane potential. The very early mitochondrial response suggests that $HgCl_2$ may target mitochondria for its toxic effect.

Conclusion

Our data indicate that the transition from the reversible stage of injury occurred simultaneously with bleb rupture and the onset of cell death, as assessed by propidium iodide uptake and loss of trapped cytoplasmic probes. A rise in cytosolic free Ca^{2+} was not the stimulus for bleb formation and was not a requirement for the progression to irreversible

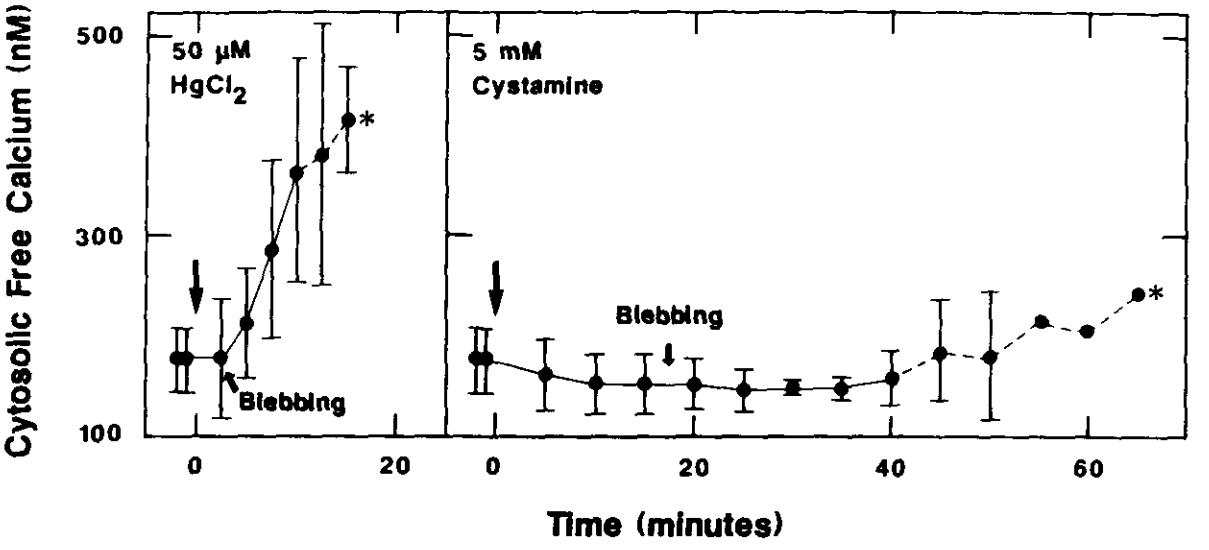

FIGURE 12. Cytosolic free Ca^{2+} with 50 μM $HgCl_2$ or 5 mM cystamine. Cytosolic free Ca^{2+} was measured in single hepatocytes using Fura-2 ratio imaging and MDVM. Cells were also examined by phase microscopy to determine the onset of blebbing, as indicated by the arrows. The dotted line in each panel represents the time period over which individual cells lost viability in each experiment. Asterisks (*) signify the time at which all cells had lost viability.

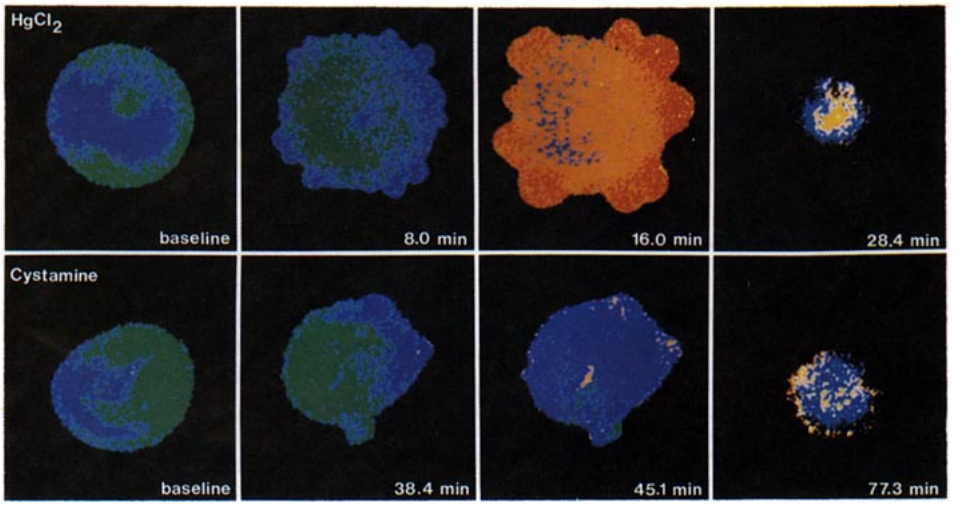

FIGURE 13. Pseudocolor map of cytosolic free Ca^{2+} after toxic injury to cultured hepatocytes. *Top*, a hepatocyte was exposed to 50 μM $HgCl_2$. *Bottom*, a hepatocyte was exposed to 5 mM cystamine. Note the increase in free Ca^{2+} after $HgCl_2$ which was especially prominent in blebs (red and yellow colors in third panel from left, top row). However, initiation of bleb formation occurred prior to the increase of free Ca^{2+} (second panel from left, top row). After cystamine, bleb formation and the onset of cell death occurred without an increase of free Ca^{2+}. The final panel in each row was taken after the cells had lost viability. These images record the weak autofluorescence of the nucleus. Cytoplasmic fluorescence above background was absent.

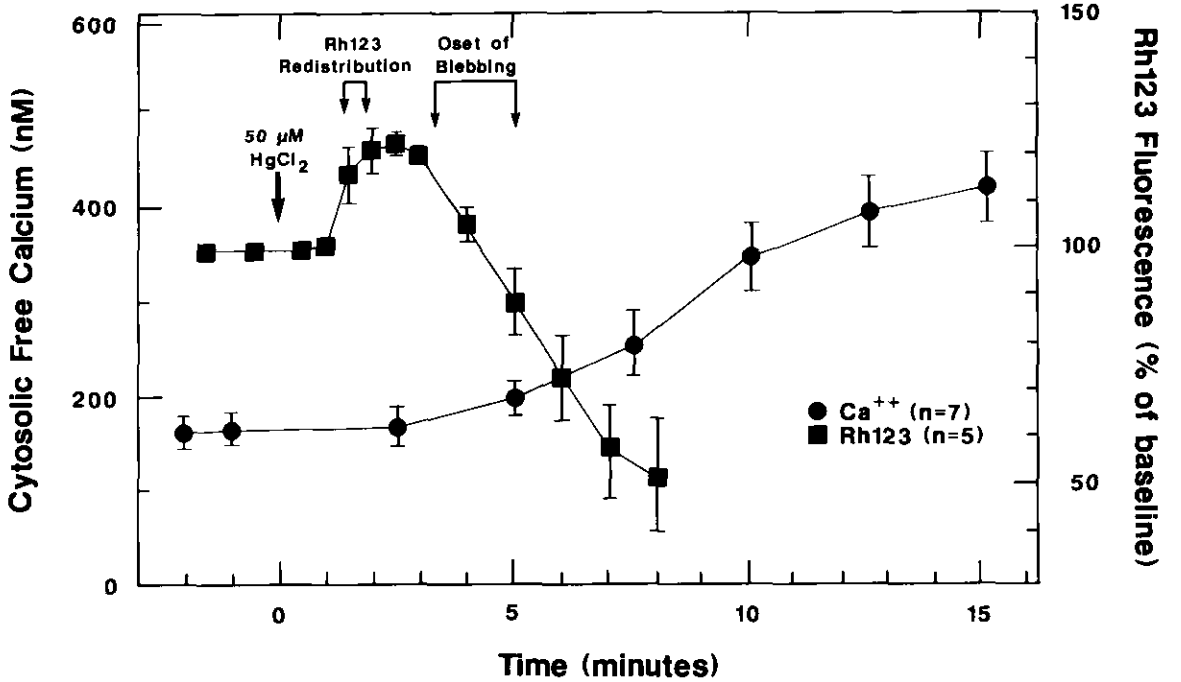

FIGURE 14. Rhodamine 123 fluorescence and cytosolic free Ca^{2+} in cultured hepatocytes after exposure to $HgCl_2$. Total cellular rhodamine 123 fluorescence and cytosolic free Ca^{2+} were determined using MDVM. Note the early increase and subsequent decrease of rhodamine 123 fluorescence that preceded the onset of blebbing and increase of cytosolic free Ca^{2+}. The increase of total cellular rhodamine 123 fluorescence is attributed to early mitochondrial depolarization. Rhodamine 123 redistributed from the mitochondrial to the cytosolic compartment with unquenching of fluorescence before exiting the cell (Fig. 11).

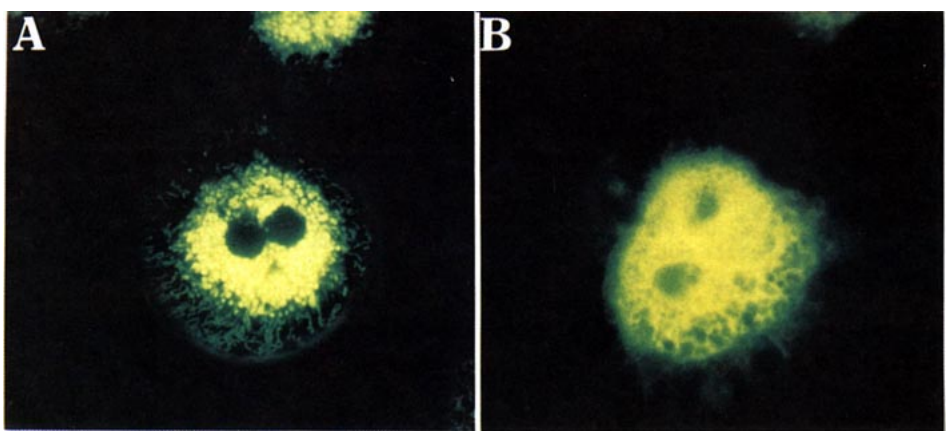

FIGURE 15. Intracellular distribution of rhodamine 123 in $HgCl_2$-treated hepatocytes. Before addition of $HgCl_2$, rhodamine 123 was localized to mitochondria (*A*). After about 2 min of exposure to 50 μM $HgCl_2$, rhodamine 123 was released from mitochondria into the cytosol (*B*). *A* and *B* show reverse images. In *A*, mitochondria are bright yellow-green spheres. In *B*, mitochondria are pale, nearly nonfluorescent spheres showing some swelling, whereas the surrounding cytoplasm is brightly fluorescent.

injury and cell death. Rather, cytosolic pH and mitochondrial membrane potential were more important factors in the progression to irreversible injury. The question remains as to how these ATP-depleted cells maintain large gradients of Ca^{2+} and hydrogen ions. The simplest explanation is that anoxia induces a large decrease of ion permeability of the plasma membrane, but the mechanisms underlying such permeability changes remain to be elucidated.

We gratefully acknowledge the expert technical assistance in electron microscopy of Mr. Yukio Tanaka.

This work was supported in part by grants HL35490, DK30874, and AG07218 from the National Institutes of Health, and a grant-in-aid from the American Heart Association, North Carolina Affiliate. G.J.G. is a recipient of an Individual National Research Service Award from the National Institutes of Health and is a Mayo Foundation Scholar.

REFERENCES

1. DiGuiseppi, J., Inman, R., Ishihara, A., Jacobson, K., and Herman, B. Applications of digitized fluorescence microscopy to problems in cell biology. BioTechniques 3: 394-403 (1985).
2. Grynkiewicz, G., Poenie, M., and Tsien, R. Y. A new generation of Ca^{++} indicators with greatly improved fluorescence properties. J. Biol. Chem. 260: 3440-3450 (1985).
3. Johnson, L. V., Walsh, M. L., Bockus, B. J., and Chen, L. B. Monitoring or relative mitochondrial membrane potential in living cells by fluorescence microscopy. J. Cell Biol. 88: 526-535 (1981).
4. Emaus, R. K., Grunwald, R., and Lemasters, J. J. Rhodamine 123 as a probe of transmembrane potential in isolated rat-liver mitochondria: spectral and metabolic properties. Biochim. Biophys. Acta 850: 436-448 (1986).
5. Bright, G. R., Fisher, G. W., Rogowska, J., and Taylor, D. L. Fluorescence ratio imaging microscopy: temporal and spatial measurements of cytoplasmic pH. J. Cell Biol. 104: 1019-1033 (1987).
6. Lemasters, J. J., DiGuiseppi, J., Nieminen, A.-L., and Herman, B. Blebbing, free Ca^{++} and mitochondrial membrane potential preceding cell death in hepatocytes. Nature 325: 78-81 (1987).
7. Lemasters, J. J. and Herman, B. Cell surface blebbing, cytosolic free calcium and mitochondrial membrane potential following toxic injury to cultured hepatocytes. J. Cell Biol. 101: 476a (1985).
8. Scanlon, M., Williams, D. A., and Fay, F. S. A Ca^{2+}-insensitive form of Fura-2 associated with polymorphonuclear leukocytes. J. Biol. Chem. 262: 6308-6312 (1987).
9. Roe, M. W. Lemasters, J. J., and Herman, B. An assessment of the use of Fura-2 or the determination of intracellular calcium concentration. Fed. Proc. 46: 227 (1987).
10. Steinberg, S. F., Bilezikian, J. P., and Al-Awqati, Q. Fura-2 fluorescence is localized to mitochondria in endothelial cells. Am. J. Physiol. 253: C744-C747 (1987).
11. Malgaroli, A., Milani, D., Meldolesi, J., and Pozzan, T. Fura-2 measurements of cytosolic free Ca^{++} in monolayers and suspensions of various types of animal cells. J. Cell Biol. 105: 2145-2155 (1987).
12. Davis, M. H., Altschuld, R. A., Jung, D.W., and Brierly, G. P. Estimation of intramitochondrial pCa and pH by Fura-2 and 2,7 biscarboxyethyl-5(6)-carboxyfluorescein (BCECF) fluorescence. Biochem. Biophys. Res. Commun. 149: 40-45 (1987).
13. Poenie, M., Alderton, J., Steinhardt, R., and Tsien, R. Calcium rises abruptly and briefly throughout the cell at the onset of anaphase. Science 233: 886-889 (1986).
14. Becker, P. L., and Fay, F. S. Photobleaching of Fura-2 and its effect on determination of calcium concentrations. Am. J. Physiol. 253: C613-C618 (1987).
15. Gores, G. J., Nieminen, A.-L., Herman, B., and Lemasters, J. J. Definitive subcellular localization of BCECF and Fura-2 in cultured hepatocytes by multiparameter digitized video microscopy. Fourth International Congress of Cell Biology. Abstracts. In press.
16. Gores, G. J., Nieminen, A.-L., Wray, B. E., Herman, B., and Lemasters, J. J. Intracellular pH during 'chemical hypoxia' in cultured rat hepatocytes: protection by intracellular-acidosis against the onset of cell death. J. Clin. Invest., submitted.
17. Herman, B., Nieminen, A.-L., Gores, G. J., and Lemasters, J. J. Irreversible injury in anoxic hepatocytes precipitated by an abrupt increase in plasma membrane permeability. FASEB J. 2: 146-151 (1988).
18. Gores, G. J., Nieminen, A.-L., Fleishman, K. E., Dawson, T. L., Herman, B., and Lemasters, J. J. Extracellular acidosis delays the onset of cell death in ATP-depleted hepatocytes. Am. J. Physiol., in press.
19. Nieminen, A.-L., Gores, G. J., Herman, B., and Lemasters, J. J. Cytosolic free Ca^{++}, mitochondrial membrane potential, cell surface blebbing and cell death in hepatocytes exposed to Hg^{++}. FASEB J. 2: A825 (1988).
20. Lemasters, J. J. Nieminen, A.-L., Gores, G. J., Wray, B. E., and Herman, B. Cytosolic free calcium and cell injury in hepatocytes. In: Cell Calcium Metabolism (G. Fiskum, Ed.), Plenum Press, New York, in press.
21. Schanne, F. A. X., Kane, A. B., Young, E. E., and Farber, J. L. Calcium dependence of toxic cell death: a final common pathway. Science 206: 700-702 (1979).
22. Trump, B. F., Berezesky, I. K., Laiho, K. U., Osornio, A. R., Mergner, W. J., and Smith, M. W. In: Scanning Electron Microscopy (A. M. R. O'Hare, Ed.), SEM Inc., Chicago, 1980, pp. 437-492.
23. Nayler, W. G. Calcium and cell death. Eur. Heart J. 4(Suppl. C): 33-41 (1983).
24. Bellomo, G., and Orrenius, S. Altered thiol and calcium homeostasis in oxidative hepatocellular injury. Hepatology 5: 876-882 (1985).
25. Hoek, J. B., Nicholls, D. G., and Williamson, J. R. Determination of the mitochondrial protonmotive force in isolated hepatocytes. J. Biol. Chem. 255: 1458-1464 (1980).
26. Andersson, B. S., Aw, T. Y., and Jones, D. P. Mitochondrial transmembrane potential and pH gradient during anoxia. Am. J. Physiol. 252: C349-C355 (1987).